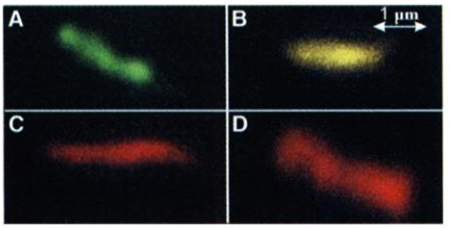

Fig. 5. Confocal microscopy images of individual nanowires with d_{TEM} = 2.5 (**A**), 3.5 (**B**), 4.2 (**C**), 5.6 nm (**D**) emitting in the green, yellow, orange, and red part of the spectrum, respectively.

length of the nanowire luminescence can be easily tuned by sizing the starting nanoparticles. With respect to the single nanowire luminescence images in Fig. 5, two points should be made: (i) The lengths of the luminescent rods in all images match very well with those seen in AFM and TEM. This means that the entire nanowire is optically active. (Some variation of the emission intensity should be attributed to confocal microscopy optics operating at high magnification.) (ii) The color of the nanowire emission remains the same over its entire length, which is reflective of the constancy of their diameter.

The described synthetic method is very simple and the quality of the produced nanowire is high. They display excellent uniformity in nanowire diameter, have a high aspect ratio, and significant quantum yield. The selection of the original particle sizes offers convenient means for the control of the degree of quantum confinement and nanowire morphology. This synthetic procedure can also be extended to other types of semiconductors: CdSe nanowires of similar dimensions and optical quality were produced in an analogous process (fig. S1), although in smaller yield. Importantly, the described process also exemplifies the ability of the nanoparticles to self-organize into a superstructure due to the intrinsic anisotropy of inter-nanoparticle interactions.

References and Notes

1. H. Dai, E. W. Wong, Y. Z. Lu, S. Fan, C. M. Lieber, *Nature* **375**, 769 (1995).
2. X. Duan, Y. Huang, Y. Cui, J. Wang, C. M. Lieber, *Nature* **409**, 66 (2001).
3. J. D. Holmes, K. P. Johnston, R. C. Doty, B. A. Korgel, *Science* **287**, 1471 (2000).
4. B. Gates, Y. Wu, Y. Yin, P. Yang, Y. Xia, *J. Am. Chem. Soc.* **123**, 11500 (2001).
5. C. R. Martin, *Science* **266**, 1961 (1994).
6. X. Peng *et al.*, *Nature* **404**, 59 (2000).
7. S. R. Nicewarner-Pena *et al.*, *Science* **294**, 137 (2001).
8. J. S. Yu *et al.*, *Chem. Commun.* 2445 (2000).
9. A. L. Rogach *et al.*, *Ber. Bunsen-Ges.* **100**, 1772 (1996).
10. A. L. Rogach, D. Nagesha, J. W. Ostrander, M. Giersig, N. A. Kotov, *Chem. Mater.* **12**, 2676 (2000).
11. L. S. Li, J. Hu, W. Yang, A. P. Alivisatos, *Nano Lett.* **1**, 349 (2001).
12. S. Takeuchi, K. Suzuki, K. Maeda, H. Iwanaga, *Philos. Mag. A* **50**, 171 (1984).
13. B. A. Korgel, D. Fitzmaurice, *Adv. Mater.* **10**, 661 (1998).
14. J. N. Wickham, A. B. Herhold, A. P. Alivisatos, *Phys. Rev. Lett.* **84**, 923 (2000).
15. M. Shim, P. Guyot-Sionnest, *J. Chem. Phys.* **111**, 6955 (1999).
16. S. A. Iakovenko *et al.*, *Adv. Mater.* **11**, 388 (1999).
17. A. Peshkovsky, A. E. McDermott, *J. Magn. Reson.* **147**, 104 (2000).
18. E. Rabani, B. Hetenyi, B. J. Berne, L. E. Brus, *J. Chem. Phys.* **110**, 5355 (1999).
19. Y. Li *et al.*, *Inorg. Chem.* **38**, 1382 (1999).
20. Y. Li *et al.*, *J. Am. Chem. Soc.* **123**, 9904 (2001).
21. The confocal optical microscopy images were processed by Leica TCS NT confocal microscopy software. 488 nm line of a water-cooled Ar-ion laser was used for luminescence excitation.
22. A. A. Mamedov, A. Belov, M. Giersig, N. N. Mamedova, N. A. Kotov, *J. Am. Chem. Soc.* **123**, 7738 (2001).
23. N.A.K. thanks the financial support of this project from NSF-CAREER (CHE-9876265), NSF-Biophotonics (BES-0119483), the Air Force Office of Scientific Research (F49620-99-C-0072), OCAST and Nomadics Inc. The authors are grateful to W. Chen for helpful advice and scientific insight. We also appreciate discussions with L. Raff from the Chemistry Department of Oklahoma State University.

Supporting Online Material

www.sciencemag.org/cgi/content/full/297/5579/237/DC1
Fig. S1
Materials and Methods

21 March 2002; accepted 2 May 2002

Role for Stearoyl-CoA Desaturase-1 in Leptin-Mediated Weight Loss

Paul Cohen,[1] Makoto Miyazaki,[5] Nicholas D. Socci,[1,2] Aaron Hagge-Greenberg,[1] Wolfgang Liedtke,[1] Alexander A. Soukas,[1] Ratnendra Sharma,[1] Lisa C. Hudgins,[3] James M. Ntambi,[5,6] Jeffrey M. Friedman[1,4]*

Leptin elicits a metabolic response that cannot be explained by its anorectic effects alone. To examine the mechanism underlying leptin's metabolic actions, we used transcription profiling to identify leptin-regulated genes in *ob/ob* liver. Leptin was found to specifically repress RNA levels and enzymatic activity of hepatic stearoyl–CoA desaturase-1 (SCD-1), which catalyzes the biosynthesis of monounsaturated fatty acids. Mice lacking SCD-1 were lean and hypermetabolic. *ob/ob* mice with mutations in SCD-1 were significantly less obese than *ob/ob* controls and had markedly increased energy expenditure. *ob/ob* mice with mutations in SCD-1 had histologically normal livers with significantly reduced triglyceride storage and VLDL (very low density lipoprotein) production. These findings suggest that down-regulation of SCD-1 is an important component of leptin's metabolic actions.

Leptin is an adipocyte-derived hormone that regulates energy balance, metabolism, and the neuroendocrine response to altered nutrition (*1, 2*). The metabolic program that leptin elicits is not explained by its effects on food intake alone (*3, 4*). Replacing leptin in leptin-deficient (*ob/ob*) mice and humans leads to the depletion of lipid in adipose tissue, liver, and other tissues (*5–8*). Leptin treatment also improves insulin sensitivity and reduces fat content in lipodystrophic mice and humans (*9, 10*).

To elucidate the mechanism by which leptin reduces hepatic lipid content, we used microarrays to identify genes in liver that were differentially regulated by leptin or by food restriction (pair-feeding). Leptin-treated *ob/ob* mice lose significantly more weight than pair-fed mice, indicating that leptin stimulates energy expenditure [fig. S1 (*11*)]. Liver RNA from these animals was hybridized to microarrays, and the data were analyzed using a *K*-means clustering algorithm (*12*). We identified 15 clusters of genes with distinct patterns of expression, six of which correspond to genes specifically regulated by leptin, but not by pair-feeding (fig. S2). To prioritize leptin-regulated genes for functional analysis, we developed an algorithm to identify and rank genes that are specifically repressed by leptin (*11*). The gene encoding SCD-1 ranked the highest in this analysis (table S1).

The microsomal enzyme SCD-1 is required for the biosynthesis of the monounsaturated fats palmitoleate and oleate from saturated fatty acids (*13, 14*). SCD-1 RNA levels were highly elevated in untreated *ob/ob* liver (Fig. 1A).

[1]Laboratory of Molecular Genetics, [2]Center for Studies in Physics and Biology, [3]Rogosin Institute, [4]Howard Hughes Medical Institute, The Rockefeller University, 1230 York Avenue, New York, NY 10021, USA. [5]Department of Biochemistry and [6]Department of Nutritional Sciences, University of Wisconsin, Madison, WI 53706, USA.

*To whom correspondence should be addressed. E-mail: friedj@rockvax.rockefeller.edu

SCD-1 RNA levels in leptin-treated *ob/ob* mice were normalized at 2 days, and by 4 days, they fell to levels below that of lean controls, a result consistent with previous studies (*15, 16*). Pair-fed mice showed a smaller and delayed decrease in SCD-1 gene expression.

SCD enzymatic activity was elevated 700% in livers of untreated *ob/ob* mice relative to wild type ($P < 0.0005$) and remained significantly elevated in saline-treated, freely fed *ob/ob* controls (Fig. 1B). Leptin treatment normalized SCD enzymatic activity, whereas pair-feeding reduced enzymatic activity to a lesser extent ($P < 0.005$ leptin versus freely fed, $P < 0.05$ leptin versus pair-fed at each time point). Levels of hepatic monounsaturated 16:1 and 18:1 fatty acids, the products of SCD-1, were elevated in *ob/ob* mice and normalized by 12 days of leptin treatment, but not by pair-feeding (table S2).

To investigate whether SCD-1 might mediate some of leptin's metabolic effects, we studied *asebia* mice (ab^J/ab^J), which carry mutations in SCD-1 (*17, 18*). The weight of male ab^J/ab^J mice was indistinguishable from that of littermates, and female ab^J/ab^J mice weighed significantly more than littermates (Fig. 2A, $P < 0.005$ at all ages after 6 weeks). However, ab^J/ab^J mice had significantly reduced fat mass relative to controls (from 12.7 to 8.3% in females, $P < 0.005$; from 13.5 to 6.9% in males, $P < 0.0005$, Fig. 2B) and plasma leptin levels (females, 2.3 ± 0.4 ng/ml versus 5.0 ± 0.9 ng/ml; males, 2.7 ± 0.5 ng/ml versus 7.8 ± 1.4 ng/ml, $P <$ 0.01 for both sexes).

To explore the effects of SCD-1 deficiency on the *ob/ob* phenotype, we intercrossed *ob/+* and $ab^J/+$ or ab^J/ab^J mice (*11*). ab^J/ab^J; *ob/ob* mice showed a dramatic reduction in body weight at all ages compared with *ob/ob* littermate controls (Fig. 2A, $P <$ 0.0001 from 5 weeks of age). At 16 weeks of age, weight was reduced by 29% in females ($P < 10^{-6}$) and 34% in males ($P < 10^{-4}$). Fat mass in 16-week-old double-mutant females was 32.1% versus 51.0% in *ob/ob* ($P < 10^{-4}$) and 28.1% in double-mutant males versus 49.9% in *ob/ob* ($P < 10^{-5}$) (Fig. 2B). ab^J/ab^J; *ob/ob* mice of both sexes also showed a significant increase in percent lean mass relative to *ob/ob* littermates (from 15.3 to 18.5% in females, $P < 0.005$; from 15.3 to 20.1% in males, $P < 0.05$), indicating that double mutants do not suffer from a generalized growth defect.

To analyze energy balance, we measured food intake and energy expenditure in *ob/ob* and lean littermates with and without homozygous SCD-1 mutations. *ob/ob* mice were hyperphagic compared with lean controls (Fig. 3, A and B). Despite being significantly leaner, ab^J/ab^J; *ob/ob* mice consumed 35% more food than *ob/ob* littermates (9.0 ± 0.9 g/day versus 6.6 ± 0.4 g/day, $P <$ 0.05) (Fig. 3, A and B). ab^J/ab^J mice consumed 53% more than lean controls (6.3 ± 0.2 g/day versus 4.2 ± 0.2 g/day, $P < 10^{-6}$) with an average food intake indistinguishable from that of *ob/ob* mice (Fig. 3, A and B). Relative to *ob/ob* controls, ab^J/ab^J; *ob/ob* mice showed increases of 96% (female) and 56% (male) in total oxygen consumption

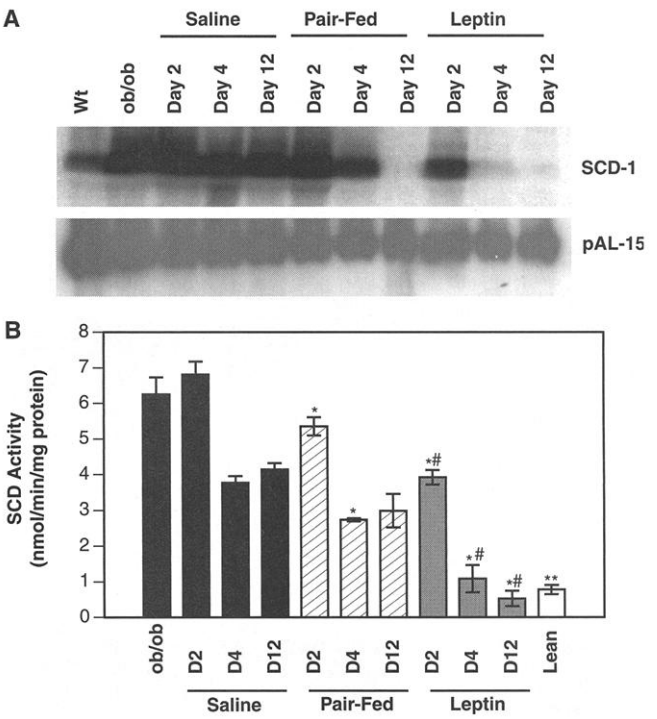

Fig. 1. Leptin-specific down-regulation of SCD-1 RNA levels and enzymatic activity. **(A)** As shown from an independent time-course experiment, Northern blots of liver RNA samples were hybridized with radioactively labeled cDNA probes specific for SCD-1 and the small mitochondrial RNA pAL-15 (loading control). **(B)** SCD enzymatic activity was measured as in (*11, 19*). Activity is expressed as nanomoles minute^{-1} milligram^{-1} protein. Error bars indicate the SEM, $n = 3$ for each group. *$P < 0.05$ versus saline treated, #$P <$ 0.05 versus pair fed, **$P <$ 0.0005 untreated lean versus untreated *ob/ob*.

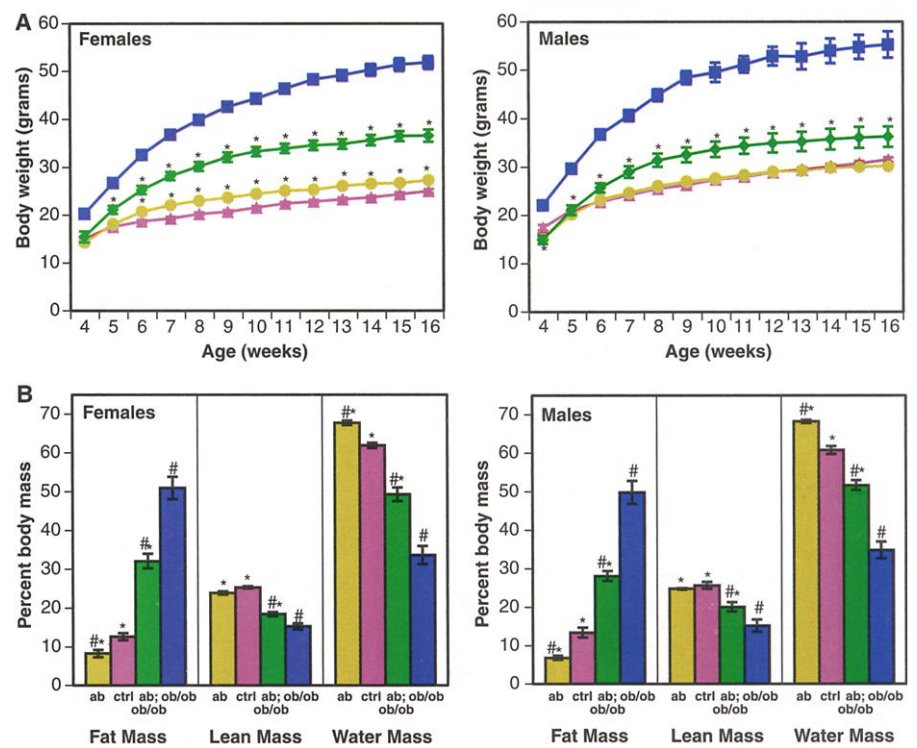

Fig. 2. Attenuation of the obese phenotype in mice with a mutation in SCD-1 (ab^J/ab^J). **(A)** Weight curves of *ob/ob* (purple squares), ab^J/ab^J; *ob/ob* (green diamonds), ab^J/ab^J (gold circles), and control (magenta triangles) mice. Error bars indicate the SEM, $n \geq 9$ for each group. *$P < 0.01$ ab^J/ab^J versus control or $P < 0.0001$ ab^J/ab^J; *ob/ob* versus *ob/ob*. **(B)** Carcass analysis of female and male *ob/ob* (purple), ab^J/ab^J; *ob/ob* (green), ab^J/ab^J (gold), and control (magenta) mice was performed as in (*11, 26*). Error bars indicate the SEM, $n \geq 8$ for each group. *$P < 0.005$ versus lean control, #$P < 0.05$ versus *ob/ob*.

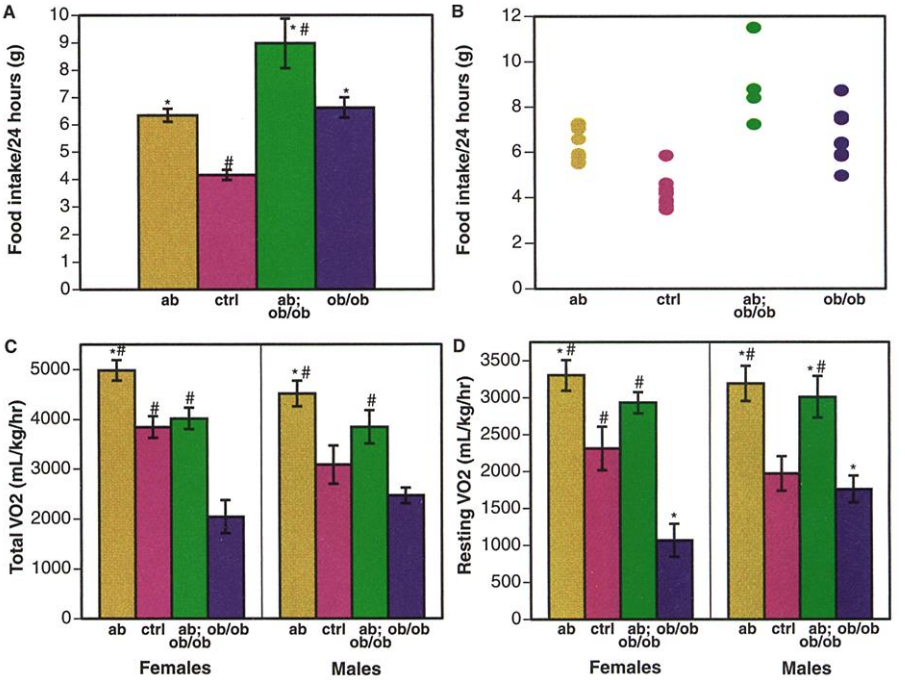

Fig. 3. Increased energy expenditure, despite persistent hyperphagia, accounts for reduced adiposity in *ab^J/ab^J; ob/ob* and *ab^J/ab^J* mice. (**A**) Average daily food intake by group and (**B**) scatterplot of average daily food intake for individual mice in each group of *ob/ob* (purple), *ab^J/ab^J; ob/ob* (green), *ab^J/ab^J* (gold), and control (magenta) mice. Mice were acclimated in individual cages and 24-hour food consumption was measured for eight consecutive days. Food intake for each mouse was averaged over the 8 days, and these values were averaged for the mice in each group. Mice were 12 to 18 weeks of age. Food intake for males and females was indistinguishable and has been pooled. Error bars indicate SEM, $n \geq 4$ for each group. $^*P < 0.05$ versus lean control, $^{\#}P < 0.05$ versus *ob/ob*. (**C**) Total and (**D**) resting oxygen consumption of female and male *ob/ob* (purple), *ab^J/ab^J; ob/ob* (green), *ab^J/ab^J* (gold), and control (magenta) mice. 14- to 16-week-old mice were placed in an Oxymax indirect calorimeter (Columbus Instruments, Columbus, OH) and allowed 2 hours to acclimate to the new environment. Measurements were taken for 5 hours during the middle of the light cycle. The total V_{O_2} is the average of these readings. The resting V_{O_2} is the average of all readings that are one standard deviation below the total V_{O_2}, as these readings represent periods of inactivity. Error bars indicate SEM, $n \geq 3$ for each group. $^*P < 0.05$ versus lean control, $^*P < 0.05$ versus *ob/ob*.

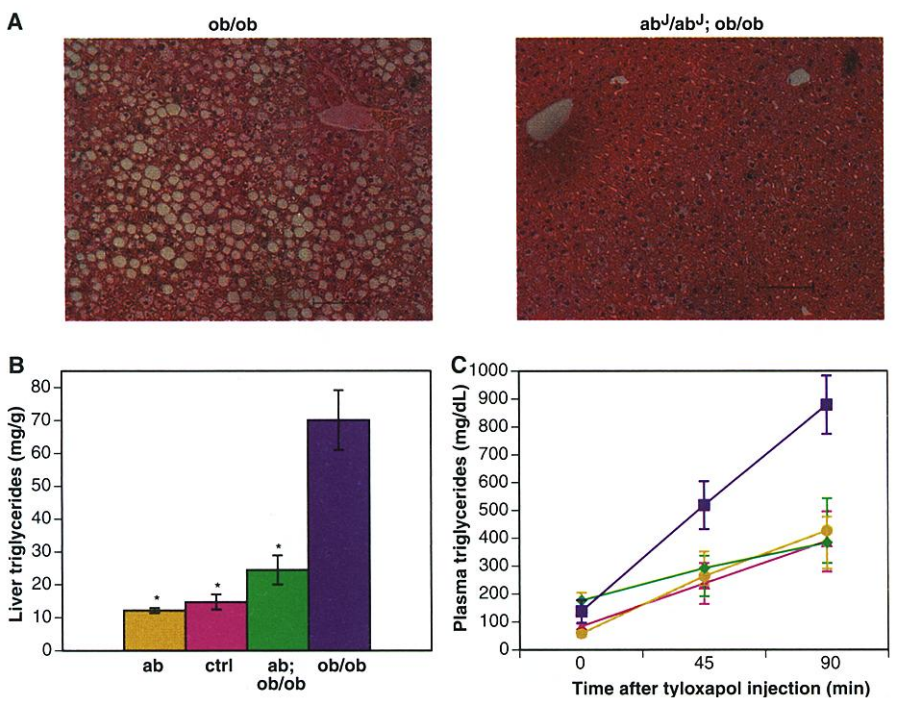

Fig. 4. Reduced hepatic lipid storage and VLDL production in *ab^J/ab^J; ob/ob* mice. (**A**) Hematoxylin and eosin (H&E)–stained liver sections from representative *ob/ob* and *ab^J/ab^J; ob/ob* mice. Images are 200× magnifications; scale bars denote 100 μm. (**B**) Liver triglyceride content of *ob/ob* (purple), *ab^J/ab^J; ob/ob* (green), *ab^J/ab^J* (gold), and control (magenta) mice. Levels were determined as in (*11, 26*). Error bars indicate SEM, $n \geq 4$ for each group. $^*P < 0.0005$ versus *ob/ob*. (**C**) VLDL production in *ob/ob* (purple), *ab^J/ab^J; ob/ob* (green), *ab^J/ab^J* (gold), and control (magenta) mice. Mice fasted for 5 hours were injected with 0.5 mg/kg tyloxapol (Triton-1339, Sigma) via the tail vein as described in (*11, 20*). Tail bleeds were done at 0, 45, and 90 min and plasma triglycerides were assayed using an enzymatic reagent. The slope of the line indicates the rate of VLDL production. Error bars indicate SEM, $n \geq 3$ for each group. For *ab^J/ab^J; ob/ob* and control, $P < 0.05$ versus *ob/ob*. For *ab^J/ab^J*, $P = 0.07$ versus *ob/ob*.

(V_{O_2}) and increases of 174% (female) and 71% (male) in resting V_{O_2} (Fig. 3, C and D; $P < 0.03$). Total and resting oxygen consumption in female double mutants were indistinguishable from those of lean controls, and in male double mutants, they were even greater than those of lean controls ($P < 0.05$ for resting V_{O_2}). Lean *ab^J/ab^J* mice expended more energy with increases of 30% and 46% in total oxygen consumption and increases of 43% and 62% in resting oxygen consumption for females and males, respectively (Fig. 3, C and D; $P < 0.02$). Double-mutant *ab^J/ab^J; ob/ob* mice had increased plasma levels of ketone bodies (β-hydroxybutyrate) relative to *ob/ob* littermates, suggesting increased fatty acid oxidation (females: 6.6 ± 1.2 mg/dl versus 3.4 ± 0.6 mg/dl; $P < 0.05$; males: 4.5 ± 1.4 mg/dl versus 3.5 ± 0.7 mg/dl; NS).

ob/ob mice have massively enlarged livers that are engorged with lipid. Gross inspection revealed that the hepatomegaly and the steatosis of *ob/ob* mice were normalized in *ab^J/ab^J; ob/ob* mice. Histological sections of *ob/ob* liver showed large lipid-filled vacuoles, whereas those of *ab^J/ab^J; ob/ob* mice showed little or no vacuolation and were indistinguishable from those of wild-type mice (Fig. 4A). The levels of liver triglyceride were substantially increased in *ob/ob* mice ($P < 0.005$ versus all other groups), whereas triglycerides in *ab^J/ab^J; ob/ob* mice were reduced to levels comparable to lean controls (Fig. 4B). As previously shown, triglyceride levels in lean *ab^J/ab^J* mice were reduced below those of lean controls (Fig. 4B) (*19*).

Palmitoleate and oleate in triglycerides and cholesteryl esters are major constituents of very low density lipoprotein (VLDL) particles, which transport fatty acids from liver to adipose tissue and other sites. We assayed the rate of hepatic lipid export in mice injected with tyloxapol, an inhibitor of VLDL hy-

drolysis, permitting the measurement of VLDL production (*20*). VLDL production was increased 140% in *ob/ob* mice relative to lean controls (Fig. 4C, $P < 0.05$). Compared with *ob/ob* controls, VLDL production was reduced 72% in ab^J/ab^J; *ob/ob* mice (8.2 mg/dl per min versus 2.3 mg/dl per min, $P < 0.02$) (Fig. 4C).

These data show that SCD-1 is required for the fully developed obese phenotype of *ob/ob* mice and suggest that a significant proportion of leptin's metabolic effects may result from inhibition of this enzyme. The basis for the metabolic effects of SCD-1 deficiency is not known. One possibility is that reduced activity of SCD-1 may decrease adiposity by decreasing cellular levels of malonyl CoA, thereby reducing fatty acid biosynthesis and de-repressing fatty acid oxidation. In the absence of SCD-1, a reduced rate of triglyceride and VLDL synthesis increases the intracellular pool of saturated fatty acyl CoAs leading to an increase in fatty acid oxidation. Monounsaturated fats are necessary for normal rates of triglyceride and cholesteryl ester synthesis, which are required for hepatic lipid storage and VLDL synthesis (*19*). Saturated fatty acyl CoAs, but not monounsaturated fatty acyl CoAs, potently allosterically inhibit acetyl-CoA carboxylase (ACC), reducing cellular levels of malonyl CoA (*21, 22*). Malonyl CoA is required for fatty acid biosynthesis and also inhibits the mitochondrial carnityl palmityl transferase shuttle system, the rate-limiting step in the import and oxidation of fatty acids in mitochondria (*23*). This putative mechanism is similar to that described in mice lacking acetyl-CoA carboxylase 2, which also have increased fatty acid oxidation in skeletal muscle and a lean phenotype (*24*). The mechanism by which leptin increases fatty acid oxidation in liver may be similar to that in skeletal muscle in that both may operate by reducing ACC activity. However, in skeletal muscle, leptin—acting directly and indirectly via the CNS—inhibits ACC via α2 AMP-kinase, which phosphorylates and inhibits ACC (*25*).

Alternative mechanisms could also account for the metabolic effects of SCD-1 deficiency. Changes in SCD-1 activity could alter the levels of ligands for peroxisome proliferator–activated receptors PPARα and PPARγ, or other nuclear hormone receptors. Changes in the ratio of saturated to unsaturated fatty acids in phospholipids can also alter membrane fluidity, which could affect signal transduction. The observed increase in energy expenditure associated with SCD-1 deficiency also suggests that uncoupling activity and/or futile cycles are induced.

The effects of leptin on SCD-1 in liver are likely to require central action, as mice lacking the leptin receptor in brain have enlarged, fatty livers, whereas livers of mice with a liver-specific knockout of the leptin receptor appear normal (*26*). Leptin also reduces hepatic SCD-1 activity when administered intracerebroventricularly (*27*). The CNS signals that modulate liver metabolism in response to leptin are unknown. SCD-1 deficiency also appears to modulate CNS pathways that regulate food intake, perhaps secondary to the increased oxygen consumption.

Leptin may also modulate the production of monounsaturated fatty acids in tissues other than liver. Down-regulation of SCD enzyme activity by leptin in other tissues, including brain, could contribute to some of the observed metabolic effects. Although SCD-1 is the only isoform normally expressed in liver, both SCD-1 and SCD-2, a similar enzyme, are expressed in most other tissues. Both enzymes catalyze the same reaction, but their cellular distribution and substrate preferences may be different.

In summary, a deficiency of SCD-1 ameliorates the obesity of *ob/ob* mice and completely corrects the hypometabolic phenotype of leptin deficiency. These findings suggest that leptin-specific down-regulation of SCD-1 is an important component of the novel metabolic response to leptin and suggests that inhibition of SCD-1 could be of benefit for the treatment of obesity, hepatic steatosis, and other metabolic disorders.

References and Notes

1. Y. Zhang *et al.*, *Nature* **372**, 425 (1994).
2. J. M. Friedman, *Nature* **404**, 632 (2000).
3. S. Kamohara, R. Burcelin, J. L. Halaas, J. M. Friedman, M. J. Charron, *Nature* **389**, 374 (1997).
4. N. Levin, C. Nelson, A. Gurney, R. Vandlen, F. de Sauvage, *Proc. Natl. Acad. Sci. U.S.A.* **93**, 1726 (1996).
5. J. L. Halaas *et al.*, *Science* **269**, 543 (1995).
6. M. A. Pelleymounter *et al.*, *Science* **269**, 540 (1995).
7. L. A. Campfield, F. J. Smith, Y. Guisez, R. Devos, P. Burn, *Science* **269**, 546 (1995).
8. I. Farooqi *et al.*, *N. Engl. J. Med.* **341**, 879 (1999).
9. I. Shimomura, R. E. Hammer, S. Ikemoto, M. S. Brown, J. L. Goldstein, *Nature* **401**, 73 (1999).
10. E. A. Oral *et al.*, *N. Engl. J. Med.* **346**, 570 (2002).
11. Materials and methods are available as supporting material on *Science* Online.
12. A. Soukas, P. Cohen, N. D. Socci, J. M. Friedman, *Genes Dev.* **14**, 963 (2000).
13. J. M. Ntambi *et al.*, *J. Biol. Chem.* **263**, 17291 (1988).
14. J. M. Ntambi, *J Lipid Res.* **40**, 1549 (1999).
15. C.-P. Liang, A. R. Tall, *J. Biol. Chem.* **276**, 49066 (2001).
16. A. W. Ferrante, M. Thearle, T. Liao, R. L. Leibel, *Diabetes* **50**, 2268 (2001).
17. A. H. Gates, M. Karasek, *Science* **148**, 1471 (1965).
18. Y. Zheng *et al.*, *Nature Genet.* **23**, 268 (1999).
19. M. Miyazaki, Y.-C. Kim, M. P. Gray-Keller, A. D. Attie, J. M. Ntambi, *J. Biol. Chem.* **275**, 30132 (2000).
20. M. Merkel *et al.*, *J. Clin. Invest.* **102**, 893 (1998).
21. J. J. Volpe, P. R. Vagelos, *Physiol. Rev.* **56**, 339 (1976).
22. M. A. Lunzer, J. A. Manning, R. K. Ockner, *J. Biol. Chem.* **252**, 5483 (1977).
23. J. D. McGarry, G. P. Mannaerts, D. W. Foster, *J. Clin. Invest.* **60**, 265 (1977).
24. L. Abu-Elheiga, M. M. Matzuk, K. A. H. Abo-Hashema, S. J. Wakil, *Science* **291**, 2613 (2001).
25. Y. Minokoshi *et al.*, *Nature* **415**, 339 (2002).
26. P. Cohen *et al.*, *J. Clin. Invest.* **108**, 1113 (2001).
27. E. Asilmaz *et al.*, unpublished observation.
28. We thank K. Mao for help with lipid quantification; T. Scase for assistance with liver histology; J. Breslow for valuable discussions and critical reading of this manuscript; E. Asilmaz, M. Ishii, J. Montez, S. Novelli, and S. Pinto for critical reading of this manuscript; and S. Korres for assistance in preparing this manuscript. Supported by NIH Medical Scientist Training Program grant GM07739 (P.C.), the American Heart Association and Xenon Genetics, Inc. (J.M.N.), and NIH grant R01-DK41096 (J.M.F.).

Supporting Online Material

www.sciencemag.org/cgi/content/full/297/5579/240/DC1
Materials and Methods
Figs. S1 and S2
Tables S1 and S2

3 March 2002; accepted 14 May 2002

Multiple Roles of *Arabidopsis VRN1* in Vernalization and Flowering Time Control

Yaron Y. Levy,* Stéphane Mesnage,*† Joshua S. Mylne, Anthony R. Gendall,‡ Caroline Dean§

***Arabidopsis VRN* genes mediate vernalization, the process by which a long period of cold induces a mitotically stable state that leads to accelerated flowering during later development. *VRN1* encodes a protein that binds DNA in vitro in a non–sequence-specific manner and functions in stable repression of the major target of the vernalization pathway, the floral repressor *FLC*. Overexpression of *VRN1* reveals a vernalization-independent function for *VRN1*, mediated predominantly through the floral pathway integrator *FT*, and demonstrates that VRN1 requires vernalization-specific factors to target *FLC*.**

Many annual plants use seasonal variations in temperature and photoperiod to control the transition to flowering (*1*). Long periods of cold temperature (1 to 3 months of about 4°C) accelerate flowering later in development in a process known as vernal-